Nonlinear dynamic substructuring in the frequency domain

Soleimani, Hossein; Aage, Niels

Published in:
Computer Methods in Applied Mechanics and Engineering

Link to article, DOI:
10.1016/j.cma.2025.117882

Publication date:
2025

Document Version
Publisher's PDF, also known as Version of record

Computer Methods in Applied Mechanics and Engineering 439 (2025) 117882

Contents lists available at ScienceDirect

Comput. Methods Appl. Mech. Engrg.

journal homepage: www.elsevier.com/locate/cma

Nonlinear dynamic substructuring in the frequency domain

Hossein Soleimani *, Niels Aage

Department of Civil and Mechanical Engineering, Technical University of Denmark, 2800, Kgs. Lyngby, Denmark
Centre for Acoustic-Mechanical Micro Systems (CAMM), Technical University of Denmark, 2800, Kgs. Lyngby, Denmark

ARTICLE INFO

Keywords:
Substructuring
Component mode synthesis
Model order reduction
Harmonic balance method

ABSTRACT

In this paper, we introduce a nonlinear dynamic substructuring technique to efficiently evaluate nonlinear systems with localized nonlinearities in the frequency domain. A closed-form equation is derived from coupling the dynamics of substructures and nonlinear connections. The method requires the linear frequency response functions of the substructures, which can be calculated independently using reduced-order methods. Increasing the number of linear bases in the reduction method for substructures does not affect the number of nonlinear equations, unlike in component mode synthesis techniques. The performance of the method is evaluated through three case studies: a lumped parameter system with cubic nonlinearity, bars with a small gap (normal contact), and a plate with a couple of nonlinear energy sinks. The results demonstrate promising accuracy with significantly reduced computational cost.

1. Introduction

Most structures consist of compound substructures that are assembled to achieve specific functionalities. This is mainly related to different production techniques and the requirement of different design expertise, such as mechanical or electrical. Therefore, the production of each component separately makes production faster and more efficient. However, to investigate the overall performance of the system, it is necessary to study the assembled structure. The study of assemblies is computationally expensive due to the high number of degrees of freedom and is even more computationally demanding with nonlinearities in the system. The nonlinear behavior can be observed even in cases where each substructure experiences small deformations at connections due to substructure contact. From a computational perspective, such as in production, it is also beneficial to examine each substructure separately and assemble them to obtain the overall response of the structure. The idea of examining assemblies component-wise has been previously addressed through domain decomposition [1], substructuring, or super element techniques [2,3].

The assembly of substructures depends on the behavior of the substructures and the type of connection, requires different techniques. Linear substructures with rigid connections can be coupled to each other using the impedance coupling method [4,5] or Lagrange multiplier frequency-based substructuring (LM-FBS) [2,6,7]. However, not all coupled systems have rigid connections. In many applications, such as spindle tool connections in machine tools, they can be modeled as elastic or viscoelastic connections. In such cases, the receptance coupling method, also known as FRF (frequency response function) coupling method, can be used [8–10]. A similar concept has also been used in enriching LM-FBS to include connection dynamics [11,12]. Despite issues arising from measurement difficulties of small amplitude degrees of freedom that are sensitive to noise [13,14], these techniques perform well. All of these methods provide a closed-form relation for the receptance of the coupled structure based on the receptance of each substructure and the dynamics of the joint. This relation shows the effect of physical parameters on the overall response and offers the opportunity to solve the equations for the dynamics of the joint and use it as an identification technique [15–18] or

* Corresponding author at: Department of Civil and Mechanical Engineering, Technical University of Denmark, 2800, Kgs. Lyngby, Denmark.
E-mail address: hsole@dtu.dk (H. Soleimani).

https://doi.org/10.1016/j.cma.2025.117882
Received 3 December 2024; Received in revised form 29 January 2025; Accepted 22 February 2025
Available online 9 March 2025

optimization. Kranjc et al. [19] eliminated the requirement of the response model of the remaining substructure in substructuring decoupling by identifying the interface forces. However, these techniques are limited to linear systems.

Nonlinearities can occur in the substructures due to geometrical or material nonlinearity, and locally in the connection [20] due to factors such as crack [21,22] or contact [23,24] or material properties of the joint, such as glue.

The concept of substructuring involving nonlinear subcomponents with rigid joints was introduced by Allen and Kuether [25,26]. They employed Nonlinear Normal Modes (NNM) [27–29] for representing each geometrically nonlinear substructure. Various reduction techniques for geometrically nonlinear structures have subsequently been developed, which can be utilized to analyze an assembled coupled structure [30–32]. An example of such a method was an extension of the Craig–Bampton method, incorporating fixed-interface nonlinear normal modes [33,34].

This paper is dedicated to applications in which the non-linearities are confined to interfaces and connections between substructures, arising from e.g contact, which in turn means that each substructure can be considered linear. Despite the confinement of the non-linearities, such situations can and will indeed render the overall response non-linear. The positive aspect of this type of nonlinearity is its localization in specific degrees of freedom within the system, primarily at joints or boundaries. As a result, we encounter a nonlinear coupled structure comprising linear substructures and nonlinear connections. To address such systems, substructuring proves beneficial, as it allows for the linear solution of larger subcomponents of the system, followed by their assembly through the nonlinear connections. However, there is no closed-form relation, analogous to linear substructuring available for nonlinear substructuring.

Segalman [35] employed the Galerkin approach to reduce the order of a coupled system by using eigenmodes of the reference linear system (RLS) and Milman–Chu Modes as basis functions. In some studies, connection nonlinearity has been modeled as a nonlinear substructure, followed by the utilization of integral equations [36] or NNM to address these nonlinear substructures [37,38]. Quinn et al. [39] decomposed the nonlinear system to a global linear system and connected an isolated nonlinear system. They used linear reduction techniques for reducing the linear system and machine learning to represent isolated nonlinear subsystem as nonlinear force acting on the main system in the time domain [40]. Kalaycıoğlu and Özgüven [41] extended the structural modification method [42] for nonlinear connections and elements for a single harmonic case. However, the proposed coupling equation includes inversion of the receptance matrix, which magnifies the noise in the case of measured FRF. On the other hand, the size of the nonlinear equations scales with the number of interested response DOFs in the system. Wei and Zheng [43] used the describing function method [44] and linear receptance to propose a multi harmonic coupling equation, which can reduce the number of nonlinear equations to $(N_h+1)\times(a+b)$, where N_h is the number of harmonics, b is nonlinear DOFs, and a is the number of interested response DOFs, thus scaling the number of nonlinear equations. However, the dominant approach for solving this type of system is Component Mode Synthesis (CMS). Component Mode Synthesis (CMS) methods [45] are well-known techniques to reduce the size of a system, and they have been widely applied in nonlinear systems [46–50]. These methods encompass substructuring, order reduction of each substructure, and assembly [51]. Methods for reducing the order of each component can be categorized into fixed interface [52], free interface [53], and mixed interface [54] methods, as well as other techniques such as the system equivalent reduction expansion process (SEREP) [55,56]. In all of these methods, the system is reduced to the number of connection degrees of freedom plus the number of modes included in each substructure. Increasing the accuracy of the solution comes at the cost of increasing the number of included mode shapes, leading to a greater number of nonlinear equations that need to be solved. After reducing the order of each component, the assembly of each substructure can be accomplished using primal or dual assembly methods [57]. Unlike linear substructuring methods, there is no closed-form equation that describes the dynamics of a coupled structure based on each component. Some research has been conducted to compare the performance of these techniques, particularly for nonlinear systems [58–60].

Another technique for modeling linear substructures with local nonlinearity is the receptance-based formulation. Menq et al. [61] developed the receptance method to study shrouded fan blade vibration in a single harmonic case. Ferreira and Ewins developed the Nonlinear Receptance Coupling Approach (NLRCA) for fundamental harmonic [62] and multi-harmonic [63] analysis based on the describing function method. More recently, Samandari and Cigeroglu [64] utilized the nonlinear receptance coupling method for computing nonlinear normal modes. Petrov [65] introduced a model reduction technique based on the receptance of the coupled structure. By partitioning the receptance matrix into linear and nonlinear degrees of freedom, the number of nonlinear equations in the system can be reduced to the nonlinear degrees of freedom. This technique, which is also addressed in Ref. [66], is more suitable for computational methods, and the receptance matrices in the equations are not related to each substructure.

This paper presents a new multi-harmonic formulation developed for nonlinear dynamic substructuring in the frequency domain. This formulation provides a closed-form relationship for the response of the coupled system based on the receptance of each substructure. It only necessitates the receptance matrix of each substructure at nonlinear, external force, and response degrees of freedom to predict the nonlinear response of the coupled structure. In other words, the method does not require a full receptance matrix for all DOFs in the system, which significantly reduces both numerical and experimental effort. Moreover, the method has no limitations on the type of nonlinearity or the number of nonlinear DOFs. By treating the relative displacement at the joint as a single coordinate, the number of nonlinear equations is condensed to half of the nonlinear degrees of freedom in the system, thereby halving the number of required nonlinear equations to be solved in the Nonlinear Receptance Coupling Approach. Even though relative displacement has been used before [46,67–69], there is no research on using that in the context of analytical and experimental substructuring. Relative displacement in the proposed method is also relaxed to undergo combined translation(s) and rotation at the coupling interface. The method requires a pair of nodes in the system to define the relative displacement and the internal action-reaction force vectors between them. This also holds for unmatched/unfitted meshes. That is, as long as it is possible to define the nonlinear element between the nodes, the method can readily be applied. However, the accuracy might be affected.

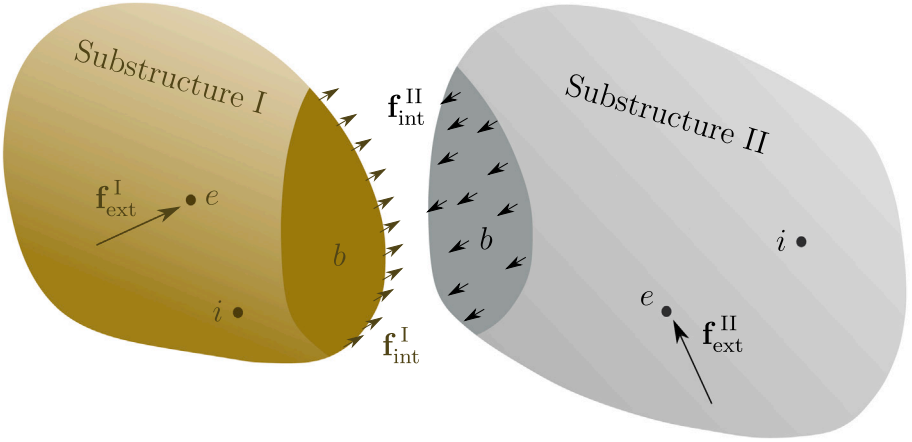

Fig. 1. Nonlinear structure composed of linear substructures and localized nonlinearity.

Not because of the nonlinear substructuring itself but due to the modeling of the nonlinearity. In such cases, it may be better to use surface-to-surface or node-to-surface methods. In other words, the proposed method is specifically applicable to node-to-node modeling approaches. Moreover, the more localized the nonlinearity, the greater is the computational advantage provided by the method. However, the formulation remains applicable even if the nonlinearity is not localized. Nonlinearities can originate from various sources, such as cracks or contact, which are modeled as nonlinear internal force vectors acting at two interfaces.

The derived closed-form equation requires the frequency response function (FRF) of each substructure at a limited number of Degrees of Freedom (DOFs) which makes it compatible with the experimental FRF of each substructure. The receptance of each substructure can be computed either computationally or experimentally. The Frequency Response Function (FRF) of each substructure can be measured through any suitable method, which is easier to conduct compared to obtaining the fixed mode shapes required in the Hurty/Craig–Bampton method. In that method, the requirement for fixed interfaces is challenging to achieve in experimental setups. Directly utilizing the FRFs also yields more accurate results in comparison to modal analysis for substructures with high damping, modal density, or specific frequency dependencies, such as rubber [2]. Clearly, the method is readily applicable to experimental measurements. However, due to length concerns, this paper is dedicated to introducing the theory and application of the technique for large computational nonlinear models. To compute the FRF, the whole dynamic stiffness matrix or block matrix can be inverted [70], or other linear reduction methods such as modal analysis or Second Order Arnoldi method (SOAR) [71] method based on the type of damping in each substructure can be used. It should be noted that the formulation is exact as long as the receptance matrix is calculated without approximation.

The structure of this manuscript is as follows: section Section 2 is dedicated to introducing the method and formulation. The verification of the method is performed in section Section 3 through three case studies, and the performance of the technique has been discussed. Finally, in section Section 4, conclusions and perspectives are made.

2. Methodology

Here, we consider a coupled structure with localized nonlinearity, which may arise from joints or cracks within the system. The coupled system can be decomposed into two substructures connected to each other through a general form of nonlinearity (see Fig. 1). After applying a spatial discretization, such as finite element, the resulting nonlinear equations of motion for the system can be represented as follows:

$$\mathbf{M}\ddot{\mathbf{x}}(t) + \mathbf{C}\dot{\mathbf{x}}(t) + \mathbf{K}\mathbf{x}(t) + \tilde{\mathbf{f}}_N(\dot{\mathbf{x}}, \mathbf{x}, t) = \tilde{\mathbf{f}}(t), \tag{1}$$

where $\mathbf{M}$, $\mathbf{C}$ and $\mathbf{K}$ are the mass, damping, and stiffness matrices of the system, respectively; $\mathbf{x}(t)$ is vector of degrees of freedom, and $\tilde{\mathbf{f}}(t)$, $\tilde{\mathbf{f}}_N(\dot{\mathbf{x}}, \mathbf{x}, t)$ are external and nonlinear force vectors of the coupled structure.

Without loss of generality, we restrict our discussion to two substructures in the following. By reordering the degrees of freedom for substructures I and II into linear (internal) DOFs (i) and nonlinear DOFs (b), while keeping in mind that the nonlinear degrees of freedom can be located anywhere within each substructure and are not restricted to the boundary (Fig. 1), we obtain:

$$\mathbf{x}^{\mathrm{I}}(t) = \begin{bmatrix} \mathbf{x}^{\mathrm{I}}_i(t) \\ \mathbf{x}^{\mathrm{I}}_b(t) \end{bmatrix}, \mathbf{x}^{\mathrm{II}}(t) = \begin{bmatrix} \mathbf{x}^{\mathrm{II}}_i(t) \\ \mathbf{x}^{\mathrm{II}}_b(t) \end{bmatrix}, \tag{2}$$

where superscript refers to substructure I and II. Inserting Eq. (2) into Eq. (1) will give decomposed nonlinear equations for each subdomain as:

$$\mathbf{M}^{\mathrm{I}} \begin{bmatrix} \ddot{\mathbf{x}}^{\mathrm{I}}_i(t) \\ \ddot{\mathbf{x}}^{\mathrm{I}}_b(t) \end{bmatrix} + \mathbf{C}^{\mathrm{I}} \begin{bmatrix} \dot{\mathbf{x}}^{\mathrm{I}}_i(t) \\ \dot{\mathbf{x}}^{\mathrm{I}}_b(t) \end{bmatrix} + \mathbf{K}^{\mathrm{I}} \begin{bmatrix} \mathbf{x}^{\mathrm{I}}_i(t) \\ \mathbf{x}^{\mathrm{I}}_b(t) \end{bmatrix} + \begin{bmatrix} \mathbf{0} \\ \tilde{\mathbf{f}}^{\mathrm{I}}_{int}(\dot{\mathbf{x}}, \mathbf{x}, t) \end{bmatrix} = \begin{bmatrix} \tilde{\mathbf{f}}^{\mathrm{I}}_i(t) \\ \tilde{\mathbf{f}}^{\mathrm{I}}_b(t) \end{bmatrix}, \tag{3}$$

$$\mathbf{M}^{\mathrm{II}}\begin{bmatrix}\ddot{\mathbf{x}}_i^{\mathrm{II}}(t)\\ \ddot{\mathbf{x}}_b^{\mathrm{II}}(t)\end{bmatrix}+\mathbf{C}^{\mathrm{II}}\begin{bmatrix}\dot{\mathbf{x}}_i^{\mathrm{II}}(t)\\ \dot{\mathbf{x}}_b^{\mathrm{II}}(t)\end{bmatrix}+\mathbf{K}^{\mathrm{II}}\begin{bmatrix}\mathbf{x}_i^{\mathrm{II}}(t)\\ \mathbf{x}_b^{\mathrm{II}}(t)\end{bmatrix}+\begin{bmatrix}\mathbf{0}\\ \tilde{\mathbf{f}}_{int}^{\mathrm{II}}(\dot{\mathbf{x}},\mathbf{x},t)\end{bmatrix}=\begin{bmatrix}\tilde{\mathbf{f}}_i^{\mathrm{II}}(t)\\ \tilde{\mathbf{f}}_b^{\mathrm{II}}(t)\end{bmatrix}. \tag{4}$$

Subdomain equations (3), (4) have two characteristics that are going to be used to reduce the number of nonlinear equations. First, nonlinearity vectors are only present in boundary DOFs because we restrict ourselves to localized nonlinearities. The second point is that these nonlinear vectors are action and reaction force as a function of relative DOFs in the system; therefore:

$$\tilde{\mathbf{f}}_{int}^{\mathrm{I}}(\dot{\mathbf{x}},\mathbf{x},t)=-\tilde{\mathbf{f}}_{int}^{\mathrm{II}}(\dot{\mathbf{x}},\mathbf{x},t)=\tilde{\mathbf{f}}_N(\dot{\mathbf{x}}_b^{\mathrm{I}}-\dot{\mathbf{x}}_b^{\mathrm{II}},\mathbf{x}_b^{\mathrm{I}}-\mathbf{x}_b^{\mathrm{II}},t). \tag{5}$$

To compute the steady-state response of the structure subjected to periodic excitation, the equations of motion will be transferred to the frequency domain. Displacements and forces are approximated using Galerkin's method with harmonic base functions using the Multi Harmonic Balance Method (MHBM) [66,72]. Following that, unknown displacements in each substructure can be expanded as:

$$\mathbf{x}^{\mathrm{I}}(t)\approx\sum_{h=0}^{n_h}\Re(\mathbf{Q}_{,h}^{\mathrm{I}}e^{jm_h\omega t}), \tag{6}$$

$$\mathbf{x}^{\mathrm{II}}(t)\approx\sum_{h=0}^{n_h}\Re(\mathbf{Q}_{,h}^{\mathrm{II}}e^{jm_h\omega t}), \tag{7}$$

where $j^2=-1$ and $\Re(\alpha)$ refers to real part of the complex number α and m_h is the selected harmonics in the response $m_h\in\{selected\ harmonics\}$ with length n_h. $\mathbf{Q}_{,h}^{\mathrm{I}}$ and $\mathbf{Q}_{,h}^{\mathrm{II}}$ are the unknown complex Fourier coefficient vectors for the system.

Due to harmonic external force and periodic expansion of the response Eqs. (6), (7), the nonlinear force vector will be approximated periodically and can be represented as:

$$\tilde{\mathbf{f}}^{\mathrm{I}}(t)\approx\sum_{h=0}^{n_h}\Re(\mathbf{F}_{,h}^{\mathrm{I}}e^{jm_h\omega t}), \tag{8}$$

$$\tilde{\mathbf{f}}^{\mathrm{II}}(t)\approx\sum_{h=0}^{n_h}\Re(\mathbf{F}_{,h}^{\mathrm{II}}e^{jm_h\omega t}), \tag{9}$$

$$\tilde{\mathbf{f}}_N(\dot{\mathbf{x}},\mathbf{x},t)\approx\sum_{h=0}^{n_h}\Re(\mathbf{f}_N^h e^{jm_h\omega t}), \tag{10}$$

where $\mathbf{F}_{,h}^{\mathrm{I}}$, $\mathbf{F}_{,h}^{\mathrm{II}}$ and $\mathbf{f}_N^h$ are Fourier coefficients of external force vectors of substructure I and II and nonlinear force vector, respectively. By inserting Eqs. (6)–(10) into the subdomain nonlinear differential equations Eqs. (3), (4) and applying Galerkin's method, the set of nonlinear algebraic equations for the unknown harmonic coefficients in the frequency domain for $h=1,2,\dots,n_h$ can be written as:

$$\begin{aligned}\mathbf{K}^{\mathrm{I}}\mathbf{Q}_{,0}^{\mathrm{I}}&=\begin{bmatrix}\mathbf{0}\\ -\mathbf{f}_N^0\end{bmatrix}+\mathbf{F}_{,0}^{\mathrm{I}},\\ (\mathbf{K}^{\mathrm{I}}+jm_h\omega\mathbf{C}^{\mathrm{I}}-(m_h\omega)^2\mathbf{M}^{\mathrm{I}})\mathbf{Q}_{,h}^{\mathrm{I}}&=\begin{bmatrix}\mathbf{0}\\ -\mathbf{f}_N^h\end{bmatrix}+\mathbf{F}_{,h}^{\mathrm{I}},\end{aligned} \tag{11}$$

$$\begin{aligned}\mathbf{K}^{\mathrm{II}}\mathbf{Q}_{,0}^{\mathrm{II}}&=\begin{bmatrix}\mathbf{0}\\ \mathbf{f}_N^0\end{bmatrix}+\mathbf{F}_{,0}^{\mathrm{II}},\\ (\mathbf{K}^{\mathrm{II}}+jm_h\omega\mathbf{C}^{\mathrm{II}}-(m_h\omega)^2\mathbf{M}^{\mathrm{II}})\mathbf{Q}_{,h}^{\mathrm{II}}&=\begin{bmatrix}\mathbf{0}\\ \mathbf{f}_N^h\end{bmatrix}+\mathbf{F}_{,h}^{\mathrm{II}},\end{aligned} \tag{12}$$

where the force coefficients for the harmonic index $m_h=0$ can be calculated as:

$$\mathbf{F}_{,h}^{\mathrm{I}}=\frac{1}{T}\int_0^T\tilde{\mathbf{f}}^{\mathrm{I}}(t)\,dt, \tag{13}$$

$$\mathbf{F}_{,h}^{\mathrm{II}}=\frac{1}{T}\int_0^T\tilde{\mathbf{f}}^{\mathrm{II}}(t)\,dt, \tag{14}$$

$$\mathbf{f}_N^h=\frac{1}{T}\int_0^T\tilde{\mathbf{f}}_N(\dot{\mathbf{x}},\mathbf{x},t)\,dt, \tag{15}$$

and the force coefficients for the rest of harmonic index h can be calculated as:

$$\mathbf{F}_{,h}^{\mathrm{I}}=\frac{2}{T}\int_0^T\tilde{\mathbf{f}}^{\mathrm{I}}(t)e^{-jm_h\omega t}\,dt, \tag{16}$$

$$\mathbf{F}_{,h}^{\mathrm{II}}=\frac{2}{T}\int_0^T\tilde{\mathbf{f}}^{\mathrm{II}}(t)e^{-jm_h\omega t}\,dt, \tag{17}$$

$$\mathbf{f}_N^h=\frac{2}{T}\int_0^T\tilde{\mathbf{f}}_N(\dot{\mathbf{x}},\mathbf{x},t)e^{-jm_h\omega t}\,dt, \tag{18}$$

in which $T = 2\pi/\omega$.

Subdomain equations (11), (12) are still coupled through the nonlinear force term. However, the left hand side of the equations are only function of each substructure without the nonlinear connection. By using this fact we can compute the receptance matrix for each substructure with free interface at the nonlinear DOFs as:

$$\mathbf{H}^{\mathrm{I}}(m_h\omega) = (\mathbf{K}^{\mathrm{I}} + jm_h\omega\mathbf{C}^{\mathrm{I}} - (m_h\omega)^2\mathbf{M}^{\mathrm{I}})^{-1}, \tag{19}$$

$$\mathbf{H}^{\mathrm{II}}(m_h\omega) = (\mathbf{K}^{\mathrm{II}} + jm_h\omega\mathbf{C}^{\mathrm{II}} - (m_h\omega)^2\mathbf{M}^{\mathrm{II}})^{-1}, \tag{20}$$

where $\mathbf{H}^{\mathrm{I}}(m_h\omega)$ and $\mathbf{H}^{\mathrm{II}}(m_h\omega)$ are the receptance matrices of substructure I and II at each harmonic, respectively. Receptance matrices depend on number of degrees of freedom and type of damping in each substructure can be calculated in different ways. Direct inversion, block matrices inversion [70], modal expansion and Second Order Arnoldi method (SOAR) [71] or experimental measurements.

By using Eqs. (19), (20) and reordering DOFs according to Eq. (2), subdomain equations (11), (12) can be written as:

$$\begin{bmatrix}\mathbf{Q}^{\mathrm{I}}_{ih}\\ \mathbf{Q}^{\mathrm{I}}_{bh}\end{bmatrix} = \begin{bmatrix}\mathbf{H}^{\mathrm{I}}_{ii}(m_h\omega) & \mathbf{H}^{\mathrm{I}}_{ib}(m_h\omega)\\ \mathbf{H}^{\mathrm{I}}_{bi}(m_h\omega) & \mathbf{H}^{\mathrm{I}}_{bb}(m_h\omega)\end{bmatrix}\begin{bmatrix}\mathbf{F}^{\mathrm{I}}_{ih}\\ -\mathbf{f}^{h}_{N} + \mathbf{F}^{\mathrm{I}}_{bh}\end{bmatrix}, \tag{21}$$

$$\begin{bmatrix}\mathbf{Q}^{\mathrm{II}}_{ih}\\ \mathbf{Q}^{\mathrm{II}}_{bh}\end{bmatrix} = \begin{bmatrix}\mathbf{H}^{\mathrm{II}}_{ii}(m_h\omega) & \mathbf{H}^{\mathrm{II}}_{ib}(m_h\omega)\\ \mathbf{H}^{\mathrm{II}}_{bi}(m_h\omega) & \mathbf{H}^{\mathrm{II}}_{bb}(m_h\omega)\end{bmatrix}\begin{bmatrix}\mathbf{F}^{\mathrm{II}}_{ih}\\ \mathbf{f}^{h}_{N} + \mathbf{F}^{\mathrm{II}}_{bh}\end{bmatrix}. \tag{22}$$

Eqs. (21), (22) are coupled through boundary/nonlinear DOFs (b). However, the nonlinear vector $\mathbf{f}^{h}_{N}$ is a function of relative displacement, therefore, the number of required nonlinear equations can be reduced by half by introducing relative displacement vector $\mathbf{q}^{h}_{rel}$ as:

$$\mathbf{q}^{h}_{rel} = \mathbf{Q}^{\mathrm{I}}_{bh} - \mathbf{Q}^{\mathrm{II}}_{bh} = \mathbf{H}^{\mathrm{I}}_{bi}(m_h\omega)\mathbf{F}^{\mathrm{I}}_{ih} + \mathbf{H}^{\mathrm{I}}_{bb}(m_h\omega)\mathbf{F}^{\mathrm{I}}_{bh} - \mathbf{H}^{\mathrm{II}}_{bi}(m_h\omega)\mathbf{F}^{\mathrm{II}}_{ih} - \mathbf{H}^{\mathrm{II}}_{bb}(m_h\omega)\mathbf{F}^{\mathrm{II}}_{bh} - (\mathbf{H}^{\mathrm{I}}_{bb}(m_h\omega) + \mathbf{H}^{\mathrm{II}}_{bb}(m_h\omega))\mathbf{f}^{h}_{N}. \tag{23}$$

In most of the systems, we have limited excitation degrees of freedom. By introducing excitation DOFs as e, Eq. (23) can be simplified to:

$$\mathbf{q}^{h}_{rel} = \mathbf{H}^{\mathrm{I}}_{be}(m_h\omega)\mathbf{F}^{\mathrm{I}}_{eh} - \mathbf{H}^{\mathrm{II}}_{be}(m_h\omega)\mathbf{F}^{\mathrm{II}}_{eh} - (\mathbf{H}^{\mathrm{I}}_{bb}(m_h\omega) + \mathbf{H}^{\mathrm{II}}_{bb}(m_h\omega))\mathbf{f}^{h}_{N}(\mathbf{q}_{rel}), \tag{24}$$

for $h = 1, 2, \ldots, n_h$ and force terms are computed using Eqs. (16)–(18). Eq. (24) provides a closed-form relation for nonlinear dynamic substructuring in the frequency domain, thereby facilitating its applicability for both computational and experimental receptance matrices. Additionally, it offers opportunities for use in identification or optimization. Remark that the experimental constitutes a significant amount of additional work and is therefore left for future work. If one of the substructures is considered rigid, the corresponding receptance matrices in Eq. (24) reduce to zero, making it applicable to structures with grounded nonlinear elements.

The procedure for using the nonlinear dynamic substructuring formulation is as follows:

- Compute, or measure, the frequency response functions (receptance matrix) for each substructure separately, at limited degrees of freedom, which are: Connection DOFs (b), external excitation DOFs (e) and interested response DOFs (r).
- Compute the external forces $\mathbf{F}^{\mathrm{I}}_{eh}$ and $\mathbf{F}^{\mathrm{II}}_{eh}$ in the frequency domain using Eqs. (16), (17). The nonlinear force term $\mathbf{f}^{h}_{N}(\mathbf{q}_{rel})$ should be calculated by selecting a model for the nonlinear connection along the parameter sweep because it depends on relative displacement using Eq. (18).
- Use Eq. (24) to couple the dynamics of two substructures with a general nonlinear connection. This equation not only couples the subdomain but also reduces the number of nonlinear equations required to half of the number of connection DOFs in the coupled structure.
- Solve the derived nonlinear complex algebraic equations using techniques such as Newton–Raphson method along with a continuation scheme [73] (Section 2.1)
- To compute the response at interested DOFs in subdomain I and II by using Eqs. (21), (22), we get:

$$\mathbf{Q}^{\mathrm{I}}_{rh} = \mathbf{H}^{\mathrm{I}}_{re}(m_h\omega)\mathbf{F}^{\mathrm{I}}_{eh} - \mathbf{H}^{\mathrm{I}}_{rb}(m_h\omega)\mathbf{f}^{h}_{N}(\mathbf{q}_{rel}), \tag{25}$$

$$\mathbf{Q}^{\mathrm{II}}_{rh} = \mathbf{H}^{\mathrm{II}}_{re}(m_h\omega)\mathbf{F}^{\mathrm{II}}_{eh} + \mathbf{H}^{\mathrm{II}}_{rb}(m_h\omega)\mathbf{f}^{h}_{N}(\mathbf{q}_{rel}), \tag{26}$$

where index (r) refers to the response degrees of freedom.

2.1. Solving the nonlinear equations

The system of nonlinear equations can be solved using various techniques which may treat the nonlinearity differently. For example, the Alternating Frequency-Time (AFT) method [74] and the Dynamic Lagrangian Frequency-Time (DLFT) method [69] are effective, with the latter being particularly well-suited for contact problems. By defining the nonlinearity through a constitutive

equation it is possible to generalize the approach for different types of nonlinearity. The integrals of nonlinear forces in the multi-harmonic balance method are computed directly, while transition points between states for nonsmooth nonlinearities are accurately determined. The condensed system of nonlinear equations (Eq. (24)) that need to be solved can be represented as a residual function as:

$$\mathbf{r}(\mathbf{q}_{rel},\omega)=\mathbf{q}_{rel}-\mathbf{p}(\omega)+\mathbf{S}(\omega)\mathbf{f}_{\mathrm{N}}(\mathbf{q}_{rel})=\mathbf{0}, \tag{27}$$

where:

$$\mathbf{q}_{rel}=[\Re(\mathbf{q}_{rel}^{1})^{\mathrm{T}},\Re(\mathbf{q}_{rel}^{2})^{\mathrm{T}},\dots,\Re(\mathbf{q}_{rel}^{n_h})^{\mathrm{T}},\Im(\mathbf{q}_{rel}^{1})^{\mathrm{T}},\Im(\mathbf{q}_{rel}^{2})^{\mathrm{T}},\dots,\Im(\mathbf{q}_{rel}^{n_h})^{\mathrm{T}}]^{\mathrm{T}}, \tag{28}$$

$$\mathbf{p}(\omega)=[\Re(\mathbf{A}_1)^{\mathrm{T}},\Re(\mathbf{A}_2)^{\mathrm{T}},\dots,\Re(\mathbf{A}_{n_h})^{\mathrm{T}},\Im(\mathbf{A}_1)^{\mathrm{T}},\Im(\mathbf{A}_2)^{\mathrm{T}},\dots,\Im(\mathbf{A}_{n_h})^{\mathrm{T}}]^{\mathrm{T}}, \tag{29}$$

in which:

$$\mathbf{A}_h(\omega)=\mathbf{H}_{be}^{\mathrm{I}}(m_h\omega)\mathbf{F}_{eh}^{\mathrm{I}}-\mathbf{H}_{be}^{\mathrm{II}}(m_h\omega)\mathbf{F}_{eh}^{\mathrm{II}}, \tag{30}$$

and in last term:

$$\mathbf{S}(\omega)=\begin{bmatrix}\Re(\mathbf{B}(\omega)) & -\Im(\mathbf{B}(\omega))\\ \Im(\mathbf{B}(\omega)) & \Re(\mathbf{B}(\omega))\end{bmatrix}, \tag{31}$$

and

$$\mathbf{f}_{\mathrm{N}}(\mathbf{q}_{rel})=[\Re(\mathbf{f}_{\mathrm{N}}^{1})^{\mathrm{T}},\Re(\mathbf{f}_{\mathrm{N}}^{2})^{\mathrm{T}},\dots,\Re(\mathbf{f}_{\mathrm{N}}^{n_h})^{\mathrm{T}},\Im(\mathbf{f}_{\mathrm{N}}^{1})^{\mathrm{T}},\Im(\mathbf{f}_{\mathrm{N}}^{2})^{\mathrm{T}},\dots,\Im(\mathbf{f}_{\mathrm{N}}^{n_h})^{\mathrm{T}}]^{\mathrm{T}}, \tag{32}$$

where:

$$\mathbf{B}(\omega)=\mathrm{diag}(\mathbf{C}_1(\omega),\mathbf{C}_2(\omega),\dots,\mathbf{C}_{n_h}(\omega)), \tag{33}$$

in which:

$$\mathbf{C}_h(\omega)=\mathbf{H}_{bb}^{\mathrm{I}}(m_h\omega)+\mathbf{H}_{bb}^{\mathrm{II}}(m_h\omega). \tag{34}$$

Here we used a prediction–correction scheme for solving the nonlinear algebraic equations. For prediction, there are different methods. The simplest continuation method is natural parameter continuation (in our case ω) or sequential scheme in which the prediction is the zero-order predictor from the previous solution point. Natural parameter continuation will fail when there are bifurcations in the system. To solve this issue, arclength s along the solution branch is used as continuation parameter i.e. $\mathbf{y}(s)=[\mathbf{q}_{rel}^{\mathrm{T}}(s),\omega(s)]^{\mathrm{T}}$. For prediction, the tangent predictor or first order predictor has been used for this problem. According to this, the prediction for the next solution point $\mathbf{y}_l^0$ is:

$$\mathbf{y}_l^0=\mathbf{y}_{l-1}+\Delta s\boldsymbol{\phi}_{l-1} \tag{35}$$

where $\mathbf{y}_{l-1}$ and $\boldsymbol{\phi}_{l-1}$ are the current converged solution point and tangent vector, respectively. Δs is the continuation step that can be chosen as a constant or as an adaptive parameter based on convergence of the response.

To find the tangent vector $\boldsymbol{\phi}(s)$ on the solution path, i.e. the derivative of the variables and parameter with respect to the continuation parameter:

$$\boldsymbol{\phi}(s)=[\mathbf{v}(s)^{\mathrm{T}},\alpha(s)]^{\mathrm{T}}=[\partial_s\mathbf{q}_{rel}^{\mathrm{T}}(s),\partial_s\omega(s)]^{\mathrm{T}}, \tag{36}$$

Eq. (27) is differentiated with respect to s and unit length implies on the tangent vector which leads to:

$$\begin{cases}\mathbf{J}_{\mathbf{q}}(\mathbf{y}(s))\mathbf{v}(s)+\mathbf{J}_{\omega}(\mathbf{y}(s))\alpha(s)=\mathbf{0},\\ \boldsymbol{\phi}(s)^{\mathrm{T}}\boldsymbol{\phi}(s)=\mathbf{v}(s)^{\mathrm{T}}\mathbf{v}(s)+\alpha(s)^2=1,\end{cases} \tag{37}$$

where:

$$\begin{aligned}\mathbf{J}_{\mathbf{q}}(\mathbf{y}(s))&=\partial_{\mathbf{q}_{rel}}\mathbf{r}(\mathbf{q}_{rel}(s),\omega(s)),\\ \mathbf{J}_{\omega}(\mathbf{y}(s))&=\partial_{\omega}\mathbf{r}(\mathbf{q}_{rel}(s),\omega(s)),\end{aligned} \tag{38}$$

which is computed by finite difference. By solving Eq. (37) analytically [75], we get:

$$\begin{aligned}\alpha(s)&=\mathrm{sign}(\det(\mathbf{J}_{\mathbf{q}}))(1+\mathbf{z}^{\mathrm{T}}\mathbf{z})^{-1/2},\\ \mathbf{v}(s)&=\alpha(s)\mathbf{z},\end{aligned} \tag{39}$$

where:

$$\mathbf{J}_{\mathbf{q}}(\mathbf{y}(s))\mathbf{z}=-\mathbf{J}_{\omega}(\mathbf{y}(s)). \tag{40}$$

The tangent vector can be computed once at the previous solution point with a pseudo-arclength continuation scheme, or approximated using finite difference relation in arclength continuation, or updated at each iteration step in the correction process as in Moore–Penrose continuation method.

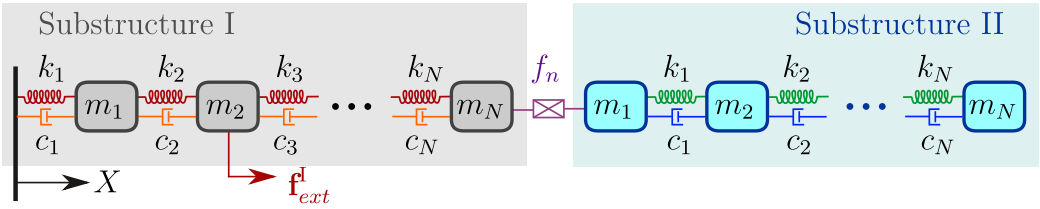

Fig. 2. Lumped parameter system with arbitrary nonlinear connection f_n.

For correction, we used the Newton–Raphson method for both variables and tangent in the Moore–Penrose continuation [76,77]:

$$\begin{aligned}\mathbf{y}_l^{j+1} &= \mathbf{y}_l^j - \begin{bmatrix}\mathbf{J_q}(\mathbf{y}_l^j) & \mathbf{J}_\omega(\mathbf{y}_l^j)\\ \left(\boldsymbol{\phi}_l^j\right)^{\mathrm{T}}\end{bmatrix}^{-1}\begin{bmatrix}\mathbf{r}(\mathbf{y}_l^j)\\ 0\end{bmatrix},\\ \boldsymbol{\phi}_l^{j+1} &= \begin{bmatrix}\mathbf{J_q}(\mathbf{y}_l^{j+1}) & \mathbf{J}_\omega(\mathbf{y}_l^{j+1})\\ \left(\boldsymbol{\phi}_l^j\right)^{\mathrm{T}}\end{bmatrix}^{-1}\begin{bmatrix}\mathbf{0}\\ 1\end{bmatrix}.\end{aligned} \tag{41}$$

for $j = 0, 1, 2, \ldots$, where $\mathbf{y}_l^0$ comes from tangent predictor (Eq. (35)) and $\boldsymbol{\phi}_l^0$ is computed by using Eqs. (36), (39) and (40) at $\mathbf{y}(s) = \mathbf{y}_{l-1}$. For tangent vector of the next step it is possible to use Eq. (39) or using updated tangent through prediction $\boldsymbol{\phi}_l = \boldsymbol{\phi}_l^{j+1}/\|\boldsymbol{\phi}_l^{j+1}\|$.

3. Numerical results

In this section, the performance of the method has been evaluated through three case studies. First case study (Section 3.1) is a lumped parameter system with strong cubic nonlinearity, which is also used for verification of the method. The second case study is two bars with a small gap in between (Section 3.2) and the last one is the evaluation of nonlinear absorber performance on a plate structure (Section 3.3). Nonlinear absorbers, which are also known as Nonlinear Energy Sink (NES) [78–80] have usually been imposed on a limited DOF system but with the help of the nonlinear dynamic substructuring technique, their performance can be evaluated in more realistic host structure with keeping the number of nonlinear equations that need to be solved to the number of absorbers in the system.

3.1. Case study i: Lumped parameter system with cubic nonlinearity

The first case study concerns two lumped parameter systems with limited degrees of freedom, connected to each other through a nonlinear element (see Fig. 2). Substructures I and II are linear with arbitrary types of damping.

Without loss of generality, we consider five degrees of freedom for substructures I and II, respectively. Substructure I has been clamped in one end, and the two substructures are connected to each other through a cubic nonlinear element with constitutive equation:

$$\bar{f}_N(x) = k_n(x + x^3) \tag{42}$$

Material parameters for substructure I and II are assumed equal and $m_i = 10$ [kg], $k_i = 1\text{e}3$ [N/m]. Both systems have structural damping which makes the stiffness matrix complex $\mathbf{K}^* = \mathbf{K}(1+i\eta)$ where $\eta = 1\text{e-}3$ and stiffness of nonlinear element is $k_n = 1\text{e}3$ [N/m]. The coupled system is excited harmonically in the second DOF of substructure I for two different force levels $f = 1, 10$ [N] and the results have been reported for the free end in substructure II (Fig. 3).

The number of nonlinear equations required to be solved for a N DOFs system with N_h harmonics included in multi harmonic balance method is $2NN_h$, whereas a coupled system with N_n nonlinear DOFs reduces to N_nN_h using the nonlinear substructuring (Eq. (24)). In the systems with localized nonlinearity $N_n \ll N$, it is a big reduction without loss of accuracy. It should be mentioned that the new nonlinear substructuring formulation is exact if the receptance has been calculated exactly. Furthermore, adding more bases in calculation of the receptance matrix for each substructure does not affect the number of nonlinear equations in the system which is the case in component mode synthesis techniques.

In Fig. 3, responses from the full nonlinear equations of motion (Eq. (1)) are compared with nonlinear substructuring relation (Eq. (24)). In this case study (Fig. 2) using 6 selected harmonics in the response, means that in the full case, 120 nonlinear equations should be solved whereas in the reduced case, the number of nonlinear equations are reduced to 12. Due to limited degrees of freedom in the system direct inversion of the matrices (Eqs. (19), (20)) is used for calculation of the receptance matrix.

Even harmonics resulting from the cubic nonlinearity in the system do not play a role in the overall response. The first 6 odd harmonic responses are depicted in Fig. 3. We expect that as the force level increases due to cubic nonlinearity, the displacement will also increase, leading to a stiffening effect and a corresponding hardening effect in the frequency response. A comparison between Fig. 3b at a high excitation force level and Fig. 3a at a lower force level clearly shows an augmentation in the hardening effect. The

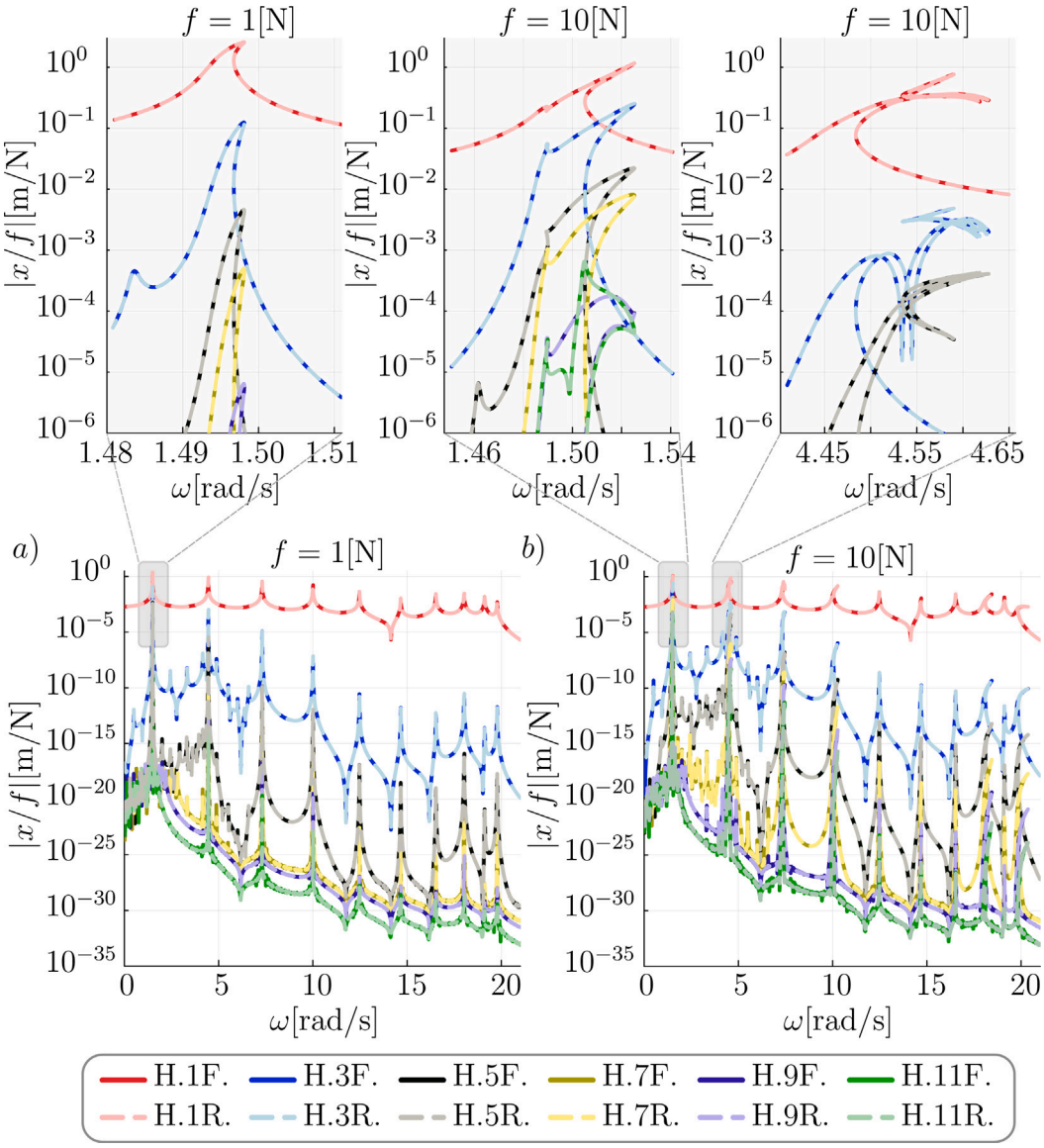

Fig. 3. Comparison of the normalized displacement for different Harmonics (H.) at free end of the structure (Fig. 2) for Reduced (R.) and Full (F.) system for force level $f = 1$ [N] (a) and for higher force level $f = 10$ [N] (b) in a wide range of frequencies.

effect of higher harmonics out of resonance is not significant. As the excitation force level increases, higher harmonics contribute more to the total response, especially around resonances. Around the second resonance at higher force levels, cross-fold bifurcation becomes evident, contrasting with the classic fold bifurcation observed around the first resonance.

Calculation time for a wide frequency range and average time per continuation step are reported in Table 1. The computational time for each continuation step is almost 10 times faster for a small lumped parameter system with 10 DOF. This speed gain will be more significant for a larger system. An adaptive solver has been used for sweeping through the frequencies and as the nonlinearity effect is more significant at higher force level, the number of continuation step increases. This is due to the fact that more iterations are needed when the nonlinearity is dominant and for higher number of unknowns in the full system. Therefore, we see large computational speed gain at higher fore level ($f = 10$ [N]) compared to lower level ($f = 1$ [N]).

3.2. Case study ii: Bars with gap

The second case study is related to studying the effect of normal contact on the dynamic response of bars. Fig. 4 demonstrates two clamped-free bars with lengths l_1 and l_2 with a small gap Δ in between which is excited harmonically at location (x_f) on the first bar.

Table 1
Computational time for calculating responses in Fig. 3.

		Time [s]	Average time per continuation step [s]
$f = 1$ [N]	Full	1873.2	0.28
	Reduced	178.8	0.04
$f = 10$ [N]	Full	8682.4	0.29
	Reduced	244.1	0.03

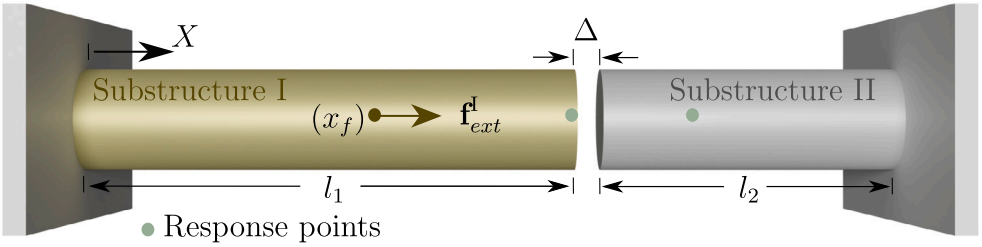

Fig. 4. Two bars with small gap in between.

This system can be seen as two linear substructures which has nonlinearity only at one degree of freedom. To be able to apply the nonlinear substructuring technique to this system, the left bar is considered as substructure I and the right bar as substructure II. The finite element method has been used for computing linear receptance matrices of each substructure separately and then coupled through the nonlinear substructuring equation (24).

The gap has been modeled by a normal contact element which can be represented as:

$$\bar{f}_N(x) = max\{0, k_c(x - \Delta)\}. \tag{43}$$

For numerical results, the following parameters has been selected, length of each bar: $l_1 = 16$ [cm], $l_2 = 10$ [cm], cross section area: $A_1 = A_2 = 1\text{e}{-4}$ [m^2], Young's modulus: $E_1 = 2$ [GPa], $E_2 = 7$ [GPa], density: $\rho_1 = 1100$ [kg/m^3], $\rho_2 = 1800$ [kg/m^3], with initial gap size: $\Delta = 100$ [μm], contact stiffness: $k_c = 1\text{e}5$ [N/m] and 320 and 200 bar elements used for discretization of substructure I and II, respectively. The calculation of receptance matrices at required DOFs has been done by modal analysis, incorporating the first 25 mode shapes in each substructure. The system has been excited harmonically in the middle of the substructure I ($x_f = 8$ [cm]), and the following results are reported at the free end of substructure I and at a distance $l_1/4 = 2.5$ [cm] from the free end in substructure II (see Fig. 4).

Fig. 5 illustrates the impact of the number of included harmonics on the first harmonic response around the first resonance of the system at an excitation force level of $f = 2$ [N]. In this case, both odd and even harmonics, along with the bias term (zero harmonic), are necessary due to the nature of the nonlinearity. The results indicate that convergence is achieved when harmonics up to the fifth order are included ($m_h = [0, 1, .., 5]$), with the relative error $\|r_{n_h+1} - r_{n_h}\|_\infty / \|r_{n_h}\|_\infty < 3\text{e} - 4$ where r_{n_h} refers to first harmonic response using n_h harmonics. A comparison of the outcomes underscores the significance of the zero harmonic in the response of the system with normal contact type nonlinearity.

The response reveals that, until reaching the point of contact, substructure I exhibits linear behavior, while substructure II remains at rest. Within the frequency range where contact is activated, the response exhibits nonlinear hardening, as illustrated in Figs. 5 and 6. This nonlinear hardening results in a shift of the resonance frequency within the system.

Table 2 shows a drastic reduction in computational time without losing the accuracy by using the nonlinear dynamic substructuring technique compared to applying the harmonic balance method directly to the full system (see Fig. 6). The nonlinear response has been calculated at the force level $f = 2$ [N] in the frequency range [12 850,13 600], using 6 harmonics ($m_h = [0, 1, .., 5]$) in the multi-harmonic balance method. All the mode shapes are included for calculating the receptance matrices in Eq. (24). In nonlinear systems with internal nonlinearity, including higher mode shapes is necessary to capture the small relative displacement between substructures. In most available reduction techniques, increasing the number of included mode shapes increases the number of nonlinear equations and correspondingly increases computational cost, whereas in the nonlinear substructuring method, the number of nonlinear equations is independent of the number of mode shapes of substructures.

Fig. 6 shows a higher harmonic response around first resonance. Higher harmonics and the response of substructure II come into play only when contact is activated in the system. As shown in Fig. 6b, the first 4 harmonics including bias term in substructure II have the same order of magnitude which demonstrate the necessity of using multi harmonic balance for getting accurate results.

The effect of excitation force level is depicted in Fig. 7. The response is calculated by including harmonics from 0 to 5 around the first resonance frequency. The responses are between two linear cases. At the lower force level $f = 0.01$ [N], the contact is not active, and substructure I behaves linearly, and the second substructure is at rest. By increasing the excitation force level, the nonlinear frequency range gets wider, and the response gets closer to a fully linear response with fully stick case with half of the stiffness of the contact.

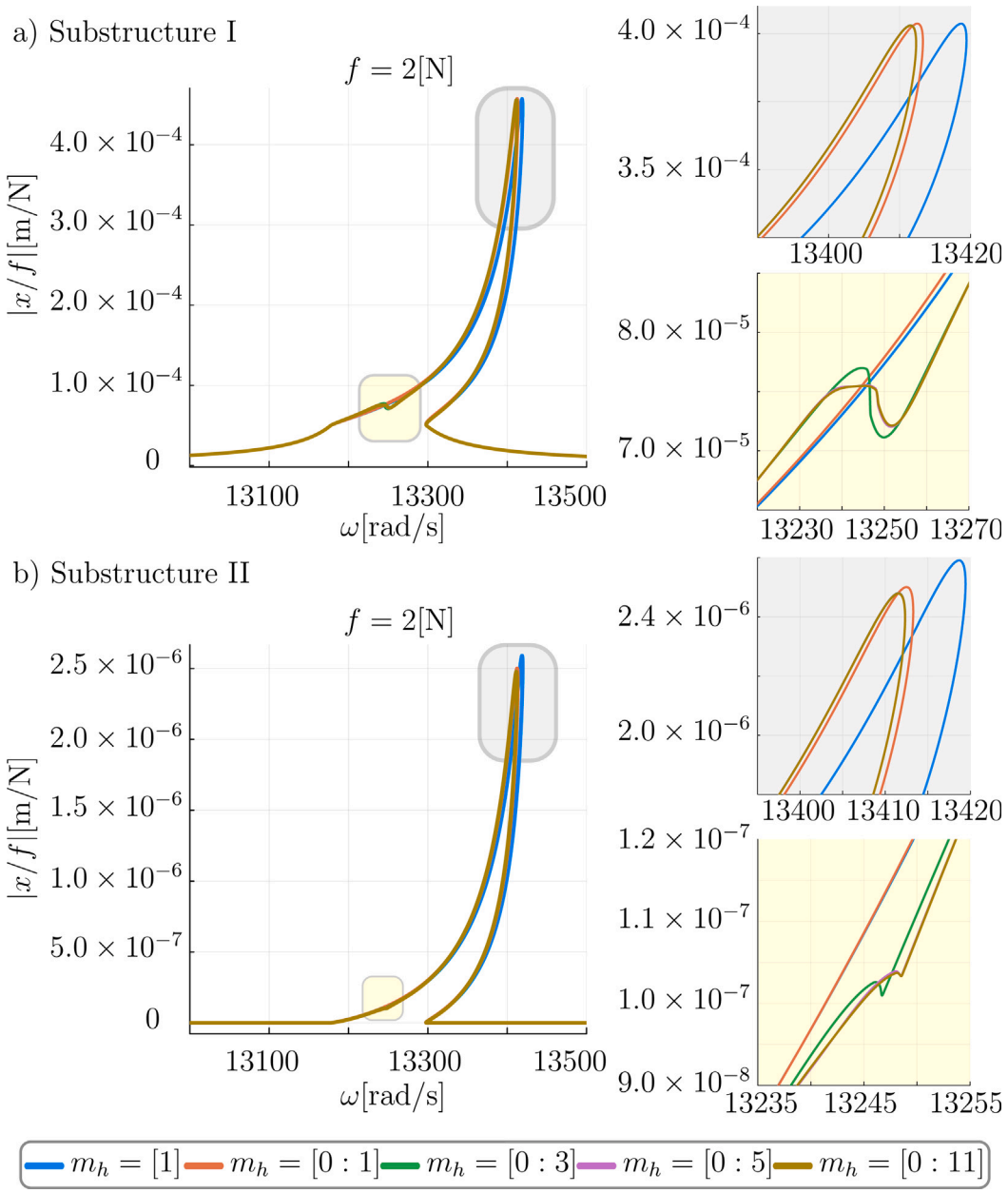

Fig. 5. Convergence of the response for substructure I (a) and substructure II (b) with respect to the number of harmonics.

Table 2
Computational time for calculating responses in second case study at the force level $f = 2$ [N] (Fig. 6).

	Time [s]	Average time per continuation step [s]
Full	248 366.0	25.23
Reduced	261.9	0.029

3.3. Case study iii: Plate with nonlinear absorbers

A dynamic absorber is a device used for reducing the vibration level of the host structure. While various types of nonlinear absorbers have been designed and studied before [79], they are predominantly implemented in systems with limited degrees of freedom. The nonlinear dynamic substructuring formulation offers the opportunity to efficiently study a large system with a limited

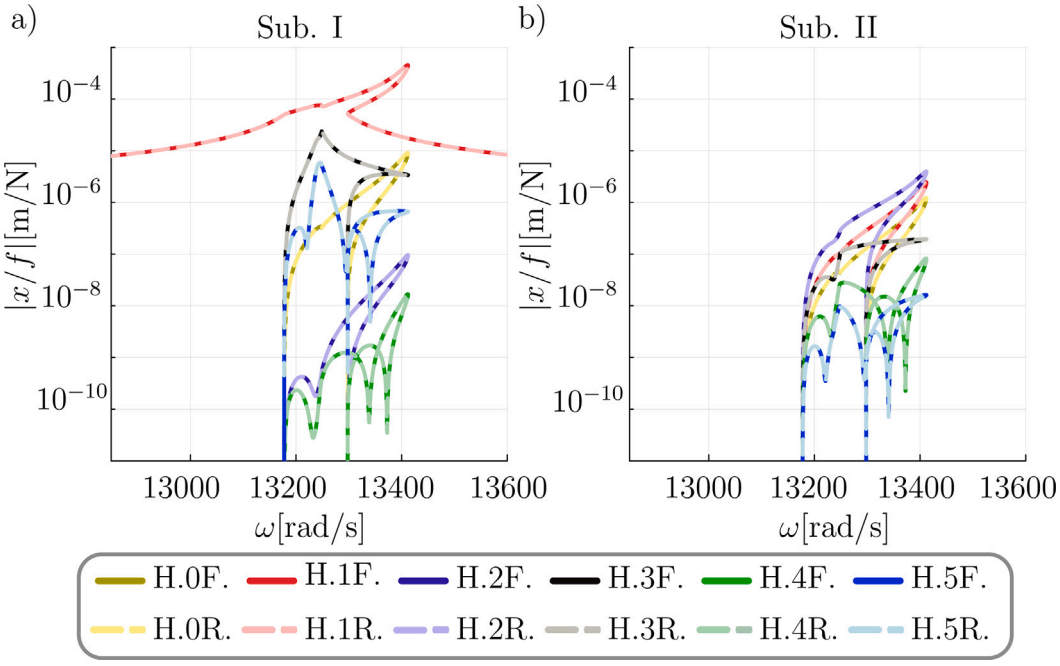

Fig. 6. Response of different Harmonics (H.) for substructure I (a) and substructure II (b) around first resonance for Reduced (R.) and Full (F.) system at the force level $f = 2$ [N].

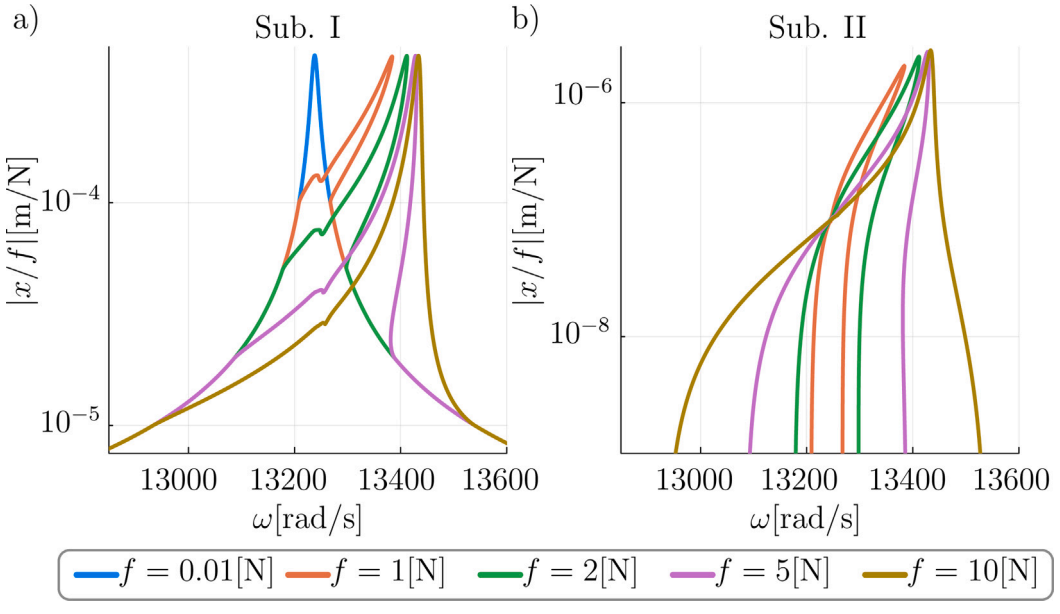

Fig. 7. Normalized first harmonic responses at substructure I (a) and substructure II (b) around first resonance for different force levels.

number of absorbers. We approach this problem by considering two substructures. Substructure I is the plate without absorbers, and substructure II comprises the masses of the absorbers connected through nonlinear absorbers. The finite element method is implemented to compute the receptance matrix of the plate for nonlinear substructuring using plate elements.

The plate with dimensions a, b and thickness h is clamped from one side (see Fig. 8) with N_a nonlinear absorbers attached to the plate at coordinate (x_i, y_i) for $i = 1, 2, \ldots, N_a$. A harmonic force is applied to the plate at coordinate (x_f, y_f). In this example, a linear spring with power law nonlinear damping is selected as a nonlinear absorber function which can be represented as:

$$\bar{f}_N^i(x) = k_i x + c_i \dot{x} \, |\dot{x}|^n \,, \tag{44}$$

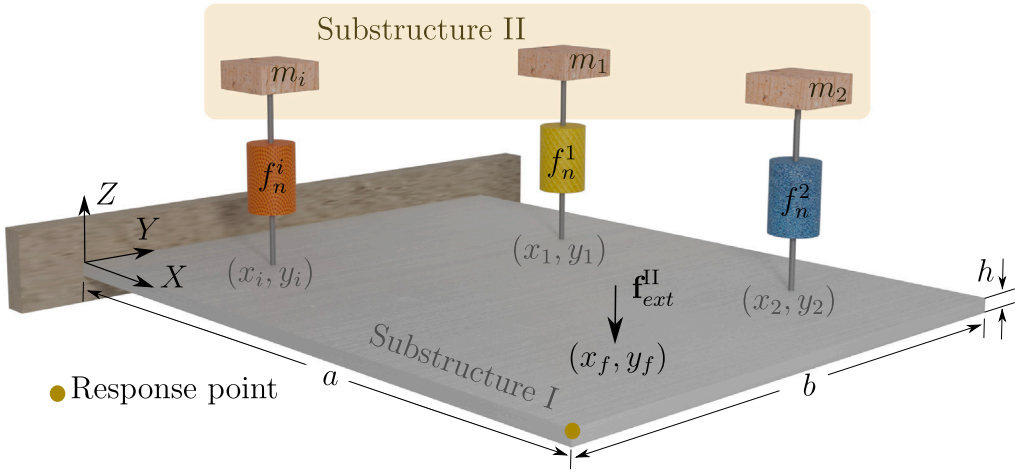

Fig. 8. Host structure (CFFF plate) with i nonlinear absorbers.

where k_i and c_i are the stiffness and damping coefficient of ith absorber. This type of nonlinearity can cover a wide range of applications such as tuned mass damper ($n = 0$), rotational inertia amplifier [81], and fluid drag force ($n = 1$).

For the numerical results, the dimensions are selected as: $a = b = 1$ [m], $h = 1$ [cm], Young's modulus $E = 70$ [GPa], density $\rho = 2710$ [kg/m^3], Poisson's ratio $\nu = 0.3$, structural damping coefficient $\eta = 1\text{e}{-3}$. 1600 Mindlin plate elements with 4 nodes per element are used to discretized the plate. Receptance matrices at required DOFs are calculated using modal analysis with all the mode shapes included. The plate is excited at the free corner $(x_f, y_f) = (a, b)$, and the results has been reported at the other free corner of the plate (see Fig. 8). The total mass ratio for the absorber is kept 5 percent of the main plate mass. In the case of more than one absorber, the total mass ratio is distributed equally among all absorbers. The mass m_i, stiffness k_i and damping coefficients c_i are tuned for targeted mode shapes with frequency ω_i based on the method in Ref. [82] for both linear and nonlinear absorber (for total mass of the plate m_t and mass ratio $\mu = 0.05$ with n absorbers: $m_i = \mu m_t/n, k_i = m_i(\frac{\omega_i}{1+\mu})^2, c_i = \sqrt{\frac{2k_i m_i \mu}{1+\mu}}$).

It should be mentioned that the stiffness and damping ratio are not optimized for the nonlinear case.

Fig. 9 demonstrates normalized first harmonic response of the plate at corner $(x_1, y_1) = (a, 0)$ with one nonlinear absorber at the mid-tip of the plate $(x_1, y_1) = (a, b/2)$. The plate is excited harmonically at the free corner $(x_f, y_f) = (a, b)$ with two excitation level $f = 1$ [N] (a) and $f = 10$ [N] (b) and in the multi-harmonic balance method, we select 5 odd harmonics, specifically $m_h = [1, 3, \ldots, 9]$, due to the odd function nonlinearity. The plots show how power n in the nonlinear constitutive equation (Eq. (44)) affects the overall response of the plate around the first resonance. The stiffness and damping coefficients k_i and c_i are tuned for the first resonance. There are two neutral points in the responses which are not affected by the change in power. The behavior of the response between these two points and outside of them is different. Between two neutral points, the nonlinear damper performs better compared to the linear damper ($n = 0$). This is due to the fact that around that region, the displacement is higher, and it produces a higher damping ratio compared to the linear case. However, outside of two neutral points, linear damping performs better and added resonances due to absorbers having smaller peaks. This might be related to the fact that the parameters are tuned for linear case to have a plateau region. By increasing the power, we see more deviation from having a plateau, which shows the necessity for changing the tuning scheme. By increasing the excitation level, the nonlinear absorber performs better due to the fact that higher level of vibration produces more damping in the system which can be seen in comparing the normalized displacements around the added resonance peaks in Fig. 9.a and .b. For instance, in the nonlinear absorbers with $n = 1$, the peak response at a force level of $f = 10$ [N] is 1.1 percent of the maximum amplitude without nonlinear absorbers, whereas at a lower force level of $f = 1$ [N], this value increases to 3.4 percent.

In Fig. 10, the effect of the number of nonlinear absorbers on the first harmonic plate response is depicted. We used the same vector of harmonics in MHBM and the plate is excited at $(x_1, y_1) = (a, b)$ with force level $f = 1$ [N]. The response is calculated at $(x_1, y_1) = (a, 0)$ and we used nonlinear absorber with power $n = 1$ in the constitutive equation (Eq. (44)). The ith absorber is tuned for the first ith resonances, for example in the case of 4 nonlinear absorbers, absorbers are tuned for resonance one to four and the location is selected according to the mode shapes as: $(x_1, y_1) = (a, b/2)$, $(x_2, y_2) = (a, 0)$, $(x_3, y_3) = (a/2, b)$, $(x_4, y_4) = (a, b)$, with the total mass ratio of 5 percent with respect to the plate which is distributed equally through all of them. As results show, targeting the first 2 resonances by two absorbers at location $(x_1, y_1) = (a, b/2)$, $(x_2, y_2) = (a, 0)$ does not have a large impact on the 3rd and 5th resonances. This is due to the type of the mode shapes, which has dominant deformation at the middle of the plate (see Fig. 10). By adding another nonlinear absorber at $(x_3, y_3) = (a/2, b)$, which is tuned for the third resonance, we could get better performance to damp the vibration around the third and fifth peak but still not a lot around the fourth resonance. Implementing a fourth absorber at coordinate $(x_4, y_4) = (a, b)$ which is tuned for fourth resonance, helps to damp all the first five peaks. Extra peaks appear in the frequency response due to extra DOF added to the system by the absorbers, but overlay compared to the base response by adding

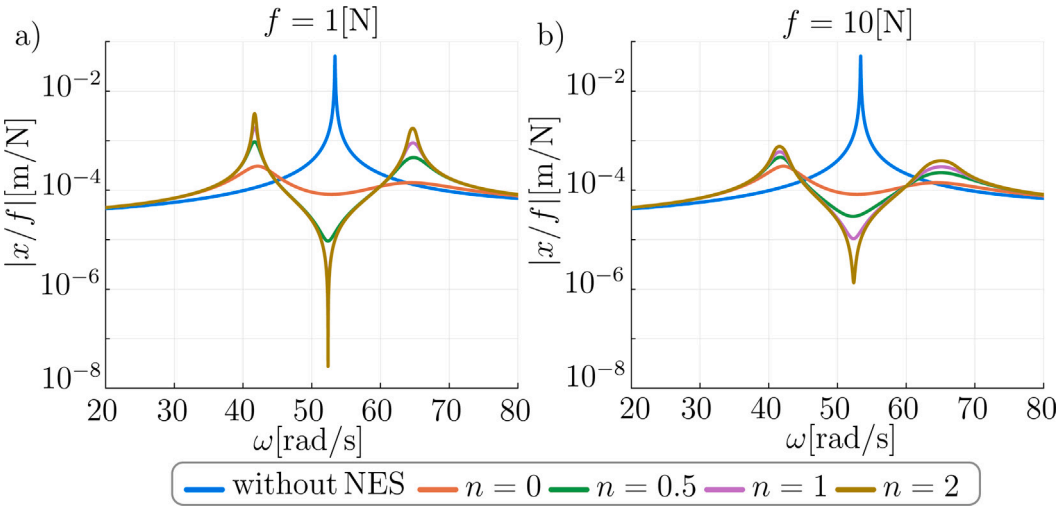

Fig. 9. Normalized first harmonic response at the free corner of the plate for two excitation level $f = 1$ [N] (a) and $f = 10$ [N] (b) with one absorber at the mid-tip of plate for different power (n) in constitutive equation around first resonance.

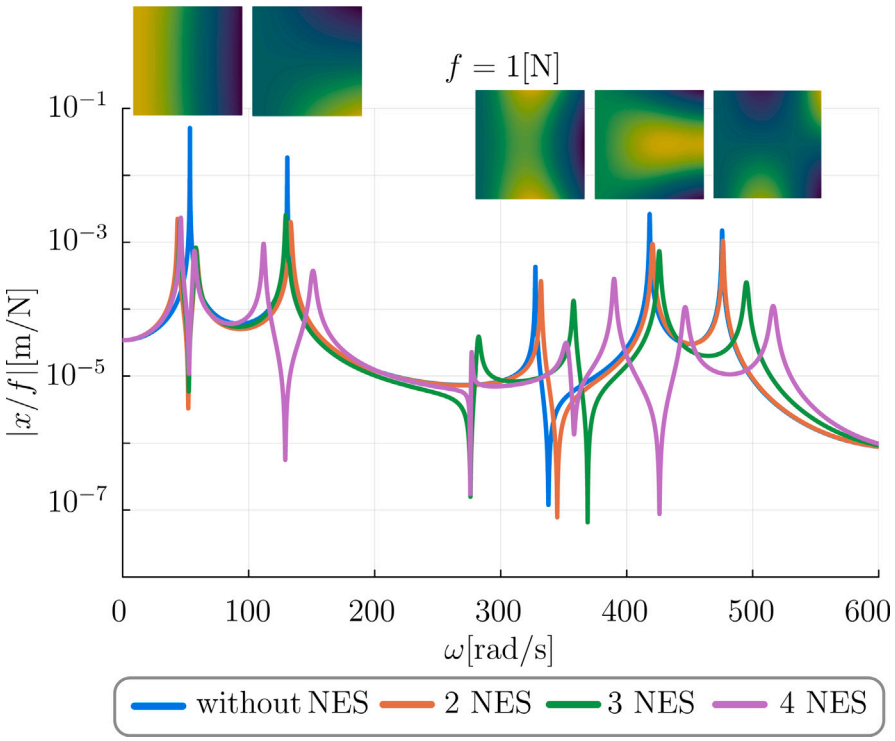

Fig. 10. Effect of number of nonlinear absorbers on the first harmonic response of the plate at force level $f = 1$ [N] and mode shapes of the plate without absorbers.

more absorbers to the system, we see better performance. The new nonlinear substructuring method makes such kind of analysis and design much faster and easier due to the limited nonlinear equations that are required to solve and makes it possible to optimize the parameters of nonlinear absorbers.

4. Conclusion

This paper presents a nonlinear dynamic substructuring method for solving nonlinear systems with localized nonlinearity in the frequency domain based on the multi-harmonic balance method. A closed-form nonlinear algebraic equation is derived, which

couples the dynamics of substructures and nonlinear connections. The coupling equation reduces the number of nonlinear equations that need to be solved to half of the number of nonlinear degrees of freedom in the system for each harmonic included in the response. The dynamics of each substructure are included by computing or measuring the receptance matrix of the linear system with a free interface. In the case of calculating the receptance matrix when the substructure is large, any linear reduction techniques such as modal analysis or Krylov subspace can be used for calculation. Using additional reduction basis vectors to improve the accuracy does not affect the number of nonlinear equations that need to be solved, which is the case in component mode synthesis techniques. The receptance matrices of substructures can also be measured through stepped sine testing at limited points in each substructure. The nonlinear substructuring relation requires the point receptance of each substructure, which is challenging to measure experimentally directly, but usually, the dynamics of the system do not change much at close points in the structure. The performance of the method has been evaluated through three case studies, which demonstrate the power of the method, especially for systems with localized nonlinearity.

CRediT authorship contribution statement

Hossein Soleimani: Writing – original draft, Visualization, Validation, Software, Methodology, Investigation, Formal analysis, Conceptualization. **Niels Aage:** Writing – review & editing, Validation, Supervision, Methodology, Formal analysis, Conceptualization.

Declaration of competing interest

The authors declare that they have no known competing financial interests or personal relationships that could have appeared to influence the work reported in this paper.

Acknowledgments

This project has received funding from hearing aid companies, including Demant, WS Audiology, and GN Resound, through the CAMM2 project (Centre for Acoustic-Mechanical Microsystems), Denmark under grant agreement No. 41-77166.

Data availability

Data will be made available on request.

References

[1] C. Gkritzalis, M. Papadrakakis, Enhanced domain decomposition Schwarz solution schemes for isogeometric collocation methods, Comput. Methods Appl. Mech. Engrg. 417 (2023) 116360, http://dx.doi.org/10.1016/j.cma.2023.116360, URL https://www.sciencedirect.com/science/article/pii/S004578252300484X, A Special Issue in Honor of the Lifetime Achievements of T. J. R. Hughes.

[2] D. de Klerk, D.J. Rixen, S.N. Voormeeren, General framework for dynamic substructuring: History, review and classification of techniques, AIAA J. 46 (5) (2008) 1169–1181, http://dx.doi.org/10.2514/1.33274.

[3] M.S. Allen, D. Rixen, M.V. der Seijs, P. Tiso, T. Abrahamsson, R.L. Mayes, Substructuring in Engineering Dynamics, Springer, 2020, http://dx.doi.org/10.1007/978-3-030-25532-9, URL https://link.springer.com/book/10.1007/978-3-030-25532-9.

[4] B. Choi, J. Park, Application of the impedance coupling method and the equivalent rotor model in rotordynamics, Finite Elem. Anal. Des. 39 (2) (2002) 93–106, http://dx.doi.org/10.1016/S0168-874X(02)00064-1, URL https://www.sciencedirect.com/science/article/pii/S0168874X02000641.

[5] J. hai Wu, A.S. Tijsseling, Y. dong Sun, Vibration analysis by impedance synthesis method of three-dimensional piping connected to a large circular cylindrical shell, Mech. Syst. Signal Process. 188 (2023) 110063, http://dx.doi.org/10.1016/j.ymssp.2022.110063, URL https://www.sciencedirect.com/science/article/pii/S0888327022011311.

[6] S.W. Klaassen, M.V. van der Seijs, D. de Klerk, System equivalent model mixing, Mech. Syst. Signal Process. 105 (2018) 90–112, http://dx.doi.org/10.1016/j.ymssp.2017.12.003, URL https://www.sciencedirect.com/science/article/pii/S0888327017306301.

[7] A. Drozg, G. Čepon, M. Boltežar, Full-degrees-of-freedom frequency based substructuring, Mech. Syst. Signal Process. 98 (2018) 570–579, http://dx.doi.org/10.1016/j.ymssp.2017.04.051, URL https://www.sciencedirect.com/science/article/pii/S088832701730273X.

[8] T. Schmitz, R. Donalson, Predicting high-speed machining dynamics by substructure analysis, CIRP Ann 49 (1) (2000) 303–308, http://dx.doi.org/10.1016/S0007-8506(07)62951-5, URL https://www.sciencedirect.com/science/article/pii/S0007850607629515.

[9] S.S. Park, Y. Altintas, M. Movahhedy, Receptance coupling for end mills, Int. J. Mach. Tools Manuf. 43 (9) (2003) 889–896, http://dx.doi.org/10.1016/S0890-6955(03)00088-9, URL https://www.sciencedirect.com/science/article/pii/S0890695503000889.

[10] A. Ertürk, H. Özgüven, E. Budak, Analytical modeling of spindle–tool dynamics on machine tools using Timoshenko beam model and receptance coupling for the prediction of tool point FRF, Int. J. Mach. Tools Manuf. 46 (15) (2006) 1901–1912, http://dx.doi.org/10.1016/j.ijmachtools.2006.01.032, URL https://www.sciencedirect.com/science/article/pii/S0890695506000484.

[11] A.E. Mahmoudi, D.J. Rixen, C.H. Meyer, Comparison of different approaches to include connection elements into frequency-based substructuring, Exp. Tech. 44 (2020) 425–433, http://dx.doi.org/10.1007/s40799-020-00360-1.

[12] V. Gimpl, A. Fantetti, S.W. Klaassen, C.W. Schwingshackl, D.J. Rixen, Contact stiffness of jointed interfaces: A comparison of dynamic substructuring techniques with frictional hysteresis measurements, Mech. Syst. Signal Process. 171 (2022) 108896, http://dx.doi.org/10.1016/j.ymssp.2022.108896, URL https://www.sciencedirect.com/science/article/pii/S088832702200084X.

[13] D. Nicgorski, P. Avitabile, Conditioning of FRF measurements for use with frequency based substructuring, Mech. Syst. Signal Process. 24 (2) (2010) 340–351, http://dx.doi.org/10.1016/j.ymssp.2009.07.013, URL https://www.sciencedirect.com/science/article/pii/S0888327009002477.

[14] F. Trainotti, M. Haeussler, D. Rixen, A practical handling of measurement uncertainties in frequency based substructuring, Mech. Syst. Signal Process. 144 (2020) 106846, http://dx.doi.org/10.1016/j.ymssp.2020.106846, URL https://www.sciencedirect.com/science/article/pii/S0888327020302326.

[15] S. Voormeeren, D. Rixen, A family of substructure decoupling techniques based on a dual assembly approach, Mech. Syst. Signal Process. 27 (2012) 379–396, http://dx.doi.org/10.1016/j.ymssp.2011.07.028, URL https://www.sciencedirect.com/science/article/pii/S0888327011003177.
[16] Ş. Tol, H.N. Özgüven, Dynamic characterization of bolted joints using FRF decoupling and optimization, Mech. Syst. Signal Process. 54–55 (2015) 124–138, http://dx.doi.org/10.1016/j.ymssp.2014.08.005, URL https://www.sciencedirect.com/science/article/pii/S0888327014003215.
[17] Z. Saeed, S.W.B. Klaassen, C.M. Firrone, T.M. Berruti, D.J. Rixen, Experimental Joint Identification Using System Equivalent Model Mixing in a Bladed Disk, J. Vib. Acoust. 142 (5) (2020) 051001, http://dx.doi.org/10.1115/1.4047361.
[18] M. Kreutz, F. Trainotti, V. Gimpl, D.J. Rixen, On the robust experimental multi-degree-of-freedom identification of bolted joints using frequency-based substructuring, Mech. Syst. Signal Process. 203 (2023) 110626, http://dx.doi.org/10.1016/j.ymssp.2023.110626, URL https://www.sciencedirect.com/science/article/pii/S0888327023005344.
[19] T. Kranjc, J. Slavič, M. Boltežar, An interface force measurements-based substructure identification and an analysis of the uncertainty propagation, Mech. Syst. Signal Process. 56–57 (2015) 2–14, http://dx.doi.org/10.1016/j.ymssp.2014.11.005, URL https://www.sciencedirect.com/science/article/pii/S0888327014004178.
[20] J. Yuan, L. Salles, F. El Haddad, C. Wong, An adaptive component mode synthesis method for dynamic analysis of jointed structure with contact friction interfaces, Comput. Struct. 229 (2020) 106177, http://dx.doi.org/10.1016/j.compstruc.2019.106177, URL https://www.sciencedirect.com/science/article/pii/S0045794919303050.
[21] J.K. Sinha, M.I. Friswell, Simulation of the dynamic response of a cracked beam, Comput. Struct. 80 (18) (2002) 1473–1476, http://dx.doi.org/10.1016/S0045-7949(02)00098-6, URL https://www.sciencedirect.com/science/article/pii/S0045794902000986.
[22] S. Bakalakos, M. Georgioudakis, M. Papadrakakis, Domain decomposition methods for 3D crack propagation problems using XFEM, Comput. Methods Appl. Mech. Engrg. 402 (2022) 115390, http://dx.doi.org/10.1016/j.cma.2022.115390, URL https://www.sciencedirect.com/science/article/pii/S0045782522004510, A Special Issue in Honor of the Lifetime Achievements of J. Tinsley Oden.
[23] M. Afzal, I. Lopez Arteaga, L. Kari, An analytical calculation of the Jacobian matrix for 3D friction contact model applied to turbine blade shroud contact, Comput. Struct. 177 (2016) 204–217, http://dx.doi.org/10.1016/j.compstruc.2016.08.014, URL https://www.sciencedirect.com/science/article/pii/S0045794916305041.
[24] A.H. Frederiksen, O. Rokoš, K. Poulios, O. Sigmund, M.G. Geers, Adding friction to Third Medium Contact: A crystal plasticity inspired approach, Comput. Methods Appl. Mech. Engrg. 432 (2024) 117412, http://dx.doi.org/10.1016/j.cma.2024.117412, URL https://www.sciencedirect.com/science/article/pii/S0045782524006674.
[25] M.S. Allen, R.J. Kuether, Substructuring with nonlinear subcomponents: a nonlinear normal mode perspective, in: Topics in Experimental Dynamics Substructuring and Wind Turbine Dynamics, Volume 2: Proceedings of the 30th IMAC, a Conference on Structural Dynamics, 2012", Springer, 2012, pp. 109–121, http://dx.doi.org/10.1007/978-1-4614-2422-2_12, URL https://link.springer.com/chapter/10.1007/978-1-4614-2422-2_12.
[26] R.J. Kuether, M.S. Allen, Nonlinear modal substructuring of systems with geometric nonlinearities, in: 54th AIAA/ASME/ASCE/AHS/ASC Structures, Structural Dynamics, and Materials Conference, 2013, p. 1521, http://dx.doi.org/10.2514/6.2013-1521, URL https://arc.aiaa.org/doi/abs/10.2514/6.2013-1521.
[27] S. Shaw, C. Pierre, Normal modes for non-linear vibratory systems, J. Sound Vib. 164 (1) (1993) 85–124, http://dx.doi.org/10.1006/jsvi.1993.1198, URL https://www.sciencedirect.com/science/article/pii/S0022460X83711983.
[28] G. Kerschen, M. Peeters, J. Golinval, A. Vakakis, Nonlinear normal modes, Part I: A useful framework for the structural dynamicist, Mech. Syst. Signal Process. 23 (1) (2009) 170–194, http://dx.doi.org/10.1016/j.ymssp.2008.04.002, URL https://www.sciencedirect.com/science/article/pii/S0888327008001015, Special Issue: Non-linear Structural Dynamics.
[29] G. Haller, S. Ponsioen, Nonlinear normal modes and spectral submanifolds: existence, uniqueness and use in model reduction, Nonlinear Dynam. 86 (2016) 1493–1534, http://dx.doi.org/10.1007/s11071-016-2974-z.
[30] L. Wu, P. Tiso, K. Tatsis, E. Chatzi, F. van Keulen, A modal derivatives enhanced rubin substructuring method for geometrically nonlinear multibody systems, Multibody Syst. Dyn. 45 (2019) 57–85, http://dx.doi.org/10.1007/s11044-018-09644-2.
[31] C. Touzé, A. Vizzaccaro, O. Thomas, Model order reduction methods for geometrically nonlinear structures: a review of nonlinear techniques, Nonlinear Dynam. 105 (2021) 1141–1190, http://dx.doi.org/10.1007/s11071-021-06693-9.
[32] Y. Shen, A. Vizzaccaro, N. Kesmia, T. Yu, L. Salles, O. Thomas, C. Touzé, Comparison of reduction methods for finite element geometrically nonlinear beam structures, Vibration 4 (1) (2021) 175–204, http://dx.doi.org/10.3390/vibration4010014, URL https://www.mdpi.com/2571-631X/4/1/14.
[33] P. Apiwattanalunggarn, S.W. Shaw, C. Pierre, Component mode synthesis using nonlinear normal modes, Nonlinear Dynam. 41 (2005) 17–46, http://dx.doi.org/10.1007/s11071-005-2791-2.
[34] R.J. Kuether, M.S. Allen, J.J. Hollkamp, Modal substructuring of geometrically nonlinear finite-element models, AIAA J. 54 (2015) 691–702, http://dx.doi.org/10.2514/1.J054036.
[35] D.J. Segalman, Model Reduction of Systems With Localized Nonlinearities, J. Comput. Nonlinear Dyn. 2 (3) (2007) 249–266, http://dx.doi.org/10.1115/1.2727495.
[36] P. Hagedorn, W. Schramm, On the Dynamics of Large Systems With Localized Nonlinearities, J. Appl. Mech. 55 (4) (1988) 946–951, http://dx.doi.org/10.1115/1.3173746.
[37] F. Latini, J. Brunetti, W. D'Ambrogio, A. Fregolent, Substructures' coupling with nonlinear connecting elements, Nonlinear Dynam. 99 (2020) 1643–1658, http://dx.doi.org/10.1007/s11071-019-05381-z.
[38] F. Latini, J. Brunetti, W. D'Ambrogio, M.S. Allen, A. Fregolent, Nonlinear substructuring in the modal domain: numerical validation and experimental verification in presence of localized nonlinearities, Nonlinear Dynam. 104 (2021) 1043–1067, http://dx.doi.org/10.1007/s11071-021-06363-w.
[39] D.D. Quinn, A.R. Brink, Global System Reduction Order Modeling for Localized Feature Inclusion, J. Vib. Acoust. 143 (4) (2020) 041006, http://dx.doi.org/10.1115/1.4048890.
[40] D.A. Najera-Flores, D.D. Quinn, A. Garland, K. Vlachas, E. Chatzi, M.D. Todd, A structure-preserving machine learning framework for accurate prediction of structural dynamics for systems with isolated nonlinearities, Mech. Syst. Signal Process. 213 (2024) 111340, http://dx.doi.org/10.1016/j.ymssp.2024.111340, URL https://www.sciencedirect.com/science/article/pii/S0888327024002383.
[41] T. Kalaycıoğlu, H.N. Özgüven, Nonlinear structural modification and nonlinear coupling, Mech. Syst. Signal Process. 46 (2) (2014) 289–306, http://dx.doi.org/10.1016/j.ymssp.2014.01.016, URL https://www.sciencedirect.com/science/article/pii/S0888327014000491.
[42] H. Nevzat Özgüven, Structural modifications using frequency response functions, Mech. Syst. Signal Process. 4 (1) (1990) 53–63, http://dx.doi.org/10.1016/0888-3270(90)90040-R, URL https://www.sciencedirect.com/science/article/pii/088832709090040R.
[43] F. Wei, G.T. Zheng, Multiharmonic Response Analysis of Systems With Local Nonlinearities Based on Describing Functions and Linear Receptance, J. Vib. Acoust. 132 (3) (2010) 031004, http://dx.doi.org/10.1115/1.4000781.
[44] O. Tanrikulu, B. Kuran, H.N. Özgüven, M. Imregun, Forced harmonic response analysis of nonlinear structures using describing functions, AIAA J. 31 (7) (1993) 1313–1320, http://dx.doi.org/10.2514/3.11769.
[45] J. Lee, M. Cho, An interpolation-based parametric reduced order model combined with component mode synthesis, Comput. Methods Appl. Mech. Engrg. 319 (2017) 258–286, http://dx.doi.org/10.1016/j.cma.2017.02.010, URL https://www.sciencedirect.com/science/article/pii/S0045782516307551.
[46] M. Krack, L. Salles, F. Thouverez, Vibration prediction of bladed disks coupled by friction joints, Arch. Comput. Methods Eng. 24 (2017) 589–636, http://dx.doi.org/10.1007/s11831-016-9183-2.

[47] S. Mehrdad Pourkiaee, S. Zucca, A Reduced Order Model for Nonlinear Dynamics of Mistuned Bladed Disks With Shroud Friction Contacts, J. Eng. Gas Turbines Power 141 (1) (2018) 011031, http://dx.doi.org/10.1115/1.4041653.
[48] M. Mitra, B.I. Epureanu, Dynamic Modeling and Projection-Based Reduction Methods for Bladed Disks With Nonlinear Frictional and Intermittent Contact Interfaces, Appl. Mech. Rev. 71 (5) (2019) 050803, http://dx.doi.org/10.1115/1.4043083.
[49] C. Monjaraz Tec, J. Gross, M. Krack, A massless boundary component mode synthesis method for elastodynamic contact problems, Comput. Struct. 260 (2022) 106698, http://dx.doi.org/10.1016/j.compstruc.2021.106698, URL https://www.sciencedirect.com/science/article/pii/S0045794921002200.
[50] L.R. Tamatam, D. Botto, S. Zucca, A coupled approach to model wear effect on shrouded bladed disk dynamics, Int. J. Mech. Sci. 237 (2023) 107816, http://dx.doi.org/10.1016/j.ijmecsci.2022.107816, URL https://www.sciencedirect.com/science/article/pii/S0020740322006968.
[51] F. Mashayekhi, A. Nobari, S. Zucca, Hybrid reduction of mistuned bladed disks for nonlinear forced response analysis with dry friction, Int. J. Non-Linear Mech. 116 (2019) 73–84, http://dx.doi.org/10.1016/j.ijnonlinmec.2019.06.001, URL https://www.sciencedirect.com/science/article/pii/S0020746219301179.
[52] R.R. Craig Jr., M.C. Bampton, Coupling of substructures for dynamic analyses, AIAA J. 6 (7) (1968) 1313–1319, http://dx.doi.org/10.2514/3.4741.
[53] S. Rubin, Improved component-mode representation for structural dynamic analysis, AIAA J. 13 (8) (1975) 995–1006, http://dx.doi.org/10.2514/3.60497.
[54] S.N. Voormeeren, P.L.C. van der Valk, D.J. Rixen, A general mixed boundary model reduction method for component mode synthesis, IOP Conf. Ser.: Mater. Sci. Eng. 10 (1) (2010) 012116, http://dx.doi.org/10.1088/1757-899X/10/1/012116.
[55] J.C. O'Callahan, System equivalent reduction expansion process, in: Proc. of the 7th Inter. Modal Analysis Conf., 1989, 1989, URL https://cir.nii.ac.jp/crid/1570572700220862208.
[56] R. Allemang, P. Avitabile, Linear modal substructuring with nonlinear connections, in: Handbook of Experimental Structural Dynamics, Springer New York, New York, NY, 2020, pp. 1–33, http://dx.doi.org/10.1007/978-1-4939-6503-8_34-1.
[57] D.J. Rixen, A dual Craig–Bampton method for dynamic substructuring, J. Comput. Appl. Math. 168 (1) (2004) 383–391, http://dx.doi.org/10.1016/j.cam.2003.12.014, URL https://www.sciencedirect.com/science/article/pii/S0377042703010045, Selected Papers from the Second International Conference on Advanced Computational Methods in Engineering (ACOMEN 2002).
[58] F.M. Gruber, D.J. Rixen, Evaluation of substructure reduction techniques with fixed and free interfaces, Strojniški Vestnik - J. Mech. Eng. 62 (7–8) (2016) 452–462, http://dx.doi.org/10.5545/sv-jme.2016.3735.
[59] J. Yuan, F. El-Haddad, L. Salles, C. Wong, Numerical Assessment of Reduced Order Modeling Techniques for Dynamic Analysis of Jointed Structures With Contact Nonlinearities, J. Eng. Gas Turbines Power 141 (3) (2018) 031027, http://dx.doi.org/10.1115/1.4041147.
[60] F. Mashayekhi, S. Zucca, A.S. Nobari, Evaluation of free interface-based reduction techniques for nonlinear forced response analysis of shrouded blades, Proc. Inst. Mech. Eng. C: J. Mech. Eng. Sci. 233 (23–24) (2019) 7459–7475, http://dx.doi.org/10.1177/0954406219872523.
[61] C.-H. Menq, J.H. Griffin, J. Bielak, The Forced Response of Shrouded Fan Stages, J. Vib. Acoust. Stress. Reliab. Des. 108 (1) (1986) 50–55, http://dx.doi.org/10.1115/1.3269303.
[62] J.V. Ferreira, D.J. Ewins, Nonlinear Receptance Coupling Approach Based on Describing Functions, SPIE INTERNATIONAL SOCIETY FOR OPTICAL, 1996, pp. 1034–1040.
[63] J.V. Ferreira, Dynamic Response Analysis of Structures with Nonlinear Components (Ph.D. thesis), Imperial College London (University of London), 1998.
[64] H. Samandari, E. Cigeroglu, A receptance based method for the calculation of nonlinear normal modes of large ordered structures with distributed localized nonlinearities, Int. J. Non-Linear Mech. 147 (2022) 104240, http://dx.doi.org/10.1016/j.ijnonlinmec.2022.104240, URL https://www.sciencedirect.com/science/article/pii/S0020746222002104.
[65] E.P. Petrov, A High-Accuracy Model Reduction for Analysis of Nonlinear Vibrations in Structures With Contact Interfaces, J. Eng. Gas Turbines Power 133 (10) (2011) 102503, http://dx.doi.org/10.1115/1.4002810.
[66] M. Krack, J. Gross, Harmonic Balance for Nonlinear Vibration Problems, vol. 1, Springer, 2019, http://dx.doi.org/10.1007/978-3-030-14023-6, URL https://link.springer.com/book/10.1007/978-3-030-14023-6#affiliations.
[67] S. Nacivet, C. Pierre, F. Thouverez, L. Jezequel, A dynamic Lagrangian frequency–time method for the vibration of dry-friction-damped systems, J. Sound Vib. 265 (1) (2003) 201–219, http://dx.doi.org/10.1016/S0022-460X(02)01447-5, URL https://www.sciencedirect.com/science/article/pii/S0022460X02014475.
[68] S.M. Pourkiaee, S. Zucca, R.G. Parker, Relative cyclic component mode synthesis: A reduced order modeling approach for mistuned bladed disks with friction interfaces, Mech. Syst. Signal Process. 163 (2022) 108197, http://dx.doi.org/10.1016/j.ymssp.2021.108197, URL https://www.sciencedirect.com/science/article/pii/S0888327021005732.
[69] T. Vadcard, A. Batailly, F. Thouverez, On harmonic balance method-based Lagrangian contact formulations for vibro-impact problems, J. Sound Vib. 531 (2022) 116950, http://dx.doi.org/10.1016/j.jsv.2022.116950, URL https://www.sciencedirect.com/science/article/pii/S0022460X22001791.
[70] T.-T. Lu, S.-H. Shiou, Inverses of 2 × 2 block matrices, Comput. Math. Appl. 43 (1) (2002) 119–129, http://dx.doi.org/10.1016/S0898-1221(01)00278-4, URL https://www.sciencedirect.com/science/article/pii/S0898122101002784.
[71] Z. Bai, Y. Su, SOAR: A second-order Arnoldi Method for the solution of the quadratic eigenvalue problem, SIAM J. Matrix Anal. Appl. 26 (3) (2005) 640–659, http://dx.doi.org/10.1137/S0895479803438523.
[72] G.-Y. Lee, Y.-H. Park, A proper generalized decomposition-based harmonic balance method with arc-length continuation for nonlinear frequency response analysis, Comput. Struct. 275 (2023) 106913, http://dx.doi.org/10.1016/j.compstruc.2022.106913, URL https://www.sciencedirect.com/science/article/pii/S0045794922001730.
[73] J. Gross, V. Gupta, C. Berthold, M. Krack, A new paradigm for multi-fidelity continuation using parallel model refinement, Comput. Methods Appl. Mech. Engrg. 423 (2024) 116860, http://dx.doi.org/10.1016/j.cma.2024.116860, URL https://www.sciencedirect.com/science/article/pii/S0045782524001166.
[74] T.M. Cameron, J.H. Griffin, An alternating frequency/time domain method for calculating the steady-state response of nonlinear dynamic systems, J. Appl. Mech. 56 (1) (1989) 149–154, http://dx.doi.org/10.1115/1.3176036, arXiv:https://asmedigitalcollection.asme.org/appliedmechanics/article-pdf/56/1/149/5460225/149_1.pdf.
[75] A. Nayfeh, B. Balachandran, Applied Nonlinear Dynamics: Analytical, Computational, and Experimental Methods, in: Wiley Series in Nonlinear Science, Wiley, 2008, URL https://books.google.dk/books?id=E2GckXZPYegC.
[76] H. Meijer, F. Dercole, B. Oldeman, Numerical bifurcation analysis, in: R.A. Meyers (Ed.), Mathematics of Complexity and Dynamical Systems, Springer New York, New York, NY, 2011, pp. 1172–1194, http://dx.doi.org/10.1007/978-1-4614-1806-1_71.
[77] T. Detroux, L. Renson, L. Masset, G. Kerschen, The harmonic balance method for bifurcation analysis of large-scale nonlinear mechanical systems, Comput. Methods Appl. Mech. Engrg. 296 (2015) 18–38, http://dx.doi.org/10.1016/j.cma.2015.07.017, URL https://www.sciencedirect.com/science/article/pii/S0045782515002297.
[78] A.F. Vakakis, O.V. Gendelman, L.A. Bergman, D.M. McFarland, G. Kerschen, Y.S. Lee, Nonlinear Targeted Energy Transfer in Mechanical and Structural Systems, vol. 156, Springer Science & Business Media, 2008, http://dx.doi.org/10.1007/978-1-4020-9130-8, URL https://link.springer.com/book/10.1007/978-1-4020-9130-8.
[79] H. Ding, L.-Q. Chen, Designs, analysis, and applications of nonlinear energy sinks, Nonlinear Dynam. 100 (2020) 3061–3107, http://dx.doi.org/10.1007/s11071-020-05724-1.
[80] A.F. Vakakis, O.V. Gendelman, L.A. Bergman, A. Mojahed, M. Gzal, Nonlinear targeted energy transfer: state of the art and new perspectives, Nonlinear Dynam. 108 (2022) 711–741, http://dx.doi.org/10.1007/s11071-022-07216-w.

[81] B. Zhao, H.R. Thomsen, X. Pu, S. Fang, Z. Lai, B.V. Damme, A. Bergamini, E. Chatzi, A. Colombi, A nonlinear damped metamaterial: Wideband attenuation with nonlinear bandgap and modal dissipation, Mech. Syst. Signal Process. 208 (2024) 111079, http://dx.doi.org/10.1016/j.ymssp.2023.111079, URL https://www.sciencedirect.com/science/article/pii/S0888327023009871.

[82] S. Krenk, J. Høgsberg, Tuned mass absorber on a flexible structure, J. Sound Vib. 333 (6) (2014) 1577–1595, http://dx.doi.org/10.1016/j.jsv.2013.11.029, URL https://www.sciencedirect.com/science/article/pii/S0022460X13009814.